LAWRENCE
LIVERMORE
NATIONAL
LABORATORY

LLNL-JRNL-811121

Phonon Dispersion of Bulk Boron-Doped Graphitic Carbon

D. McGlamery, A. A. Baker, M. A. Mosquera, N. P. Stadie

June 2, 2020

Journal of Physical Chemistry C

Disclaimer

This document was prepared as an account of work sponsored by an agency of the United States government. Neither the United States government nor Lawrence Livermore National Security, LLC, nor any of their employees makes any warranty, expressed or implied, or assumes any legal liability or responsibility for the accuracy, completeness, or usefulness of any information, apparatus, product, or process disclosed, or represents that its use would not infringe privately owned rights. Reference herein to any specific commercial product, process, or service by trade name, trademark, manufacturer, or otherwise does not necessarily constitute or imply its endorsement, recommendation, or favoring by the United States government or Lawrence Livermore National Security, LLC. The views and opinions of authors expressed herein do not necessarily state or reflect those of the United States government or Lawrence Livermore National Security, LLC, and shall not be used for advertising or product endorsement purposes.

Phonon Dispersion Relation of Bulk Boron-Doped Graphitic Carbon

Devin McGlamery†, Alexander A. Baker‡, Yi-Sheng Liu‖, Martín A. Mosquera†, and Nicholas P. Stadie†*

†Department of Chemistry & Biochemistry, Montana State University, Bozeman, Montana, 59717, United States

‡Materials Science Division, Lawrence Livermore National Laboratory, Livermore, California, 94550, United States

‖Advanced Light Source, Lawrence Berkeley National Laboratory, Berkeley, California, 94720, United States

KEYWORDS: Boron, Carbonaceous, Turbostratic Graphite, Raman Spectroscopy, X-Ray Diffraction, X-Ray Absorption Spectroscopy, Vibrational Structure, Substitutional Doping, Solid Solution.

ABSTRACT: Bulk turbostratic graphitic carbon of varying levels of disorder and chemical composition have been synthesized by a direct synthesis method in the temperature range of 750 °C to 1100 °C, with a focus on boron incorporation within the graphitic lattice. The atomistic and electronic/vibrational structure were characterized by X-ray diffraction, energy dispersive X-ray spectroscopy, Auger electron spectroscopy, X-ray absorption spectroscopy, and Raman spectroscopy. The phonon dispersion relation of graphitic carbon was found to be uniquely sensitive to substitutional boron doping, which perturbs the phonon structure while leaving the lattice structure unchanged. The dispersion relation of the D peak measured by Raman spectroscopy can be used to uniquely identify bulk graphitic materials that containing a large content of ordered trigonal planar g-BC_3 units, which are of high interest in applications ranging from hydrogen storage to lithium-ion batteries.

INTRODUCTION

Substitutional boron doping of graphite has proven to be an effective method to improve thermoelectric power[1], oxidation resistance[2-5], the capture of thermal neutrons[6], and the ability to accept alkali metal intercalants (e.g., Li, Na, and K)[7-11]. Numerous theoretical studies have shown great promise for high boron-content graphitic solutions, notably BC_3 (25 at. % boron), as an electrode material in electrochemical energy storage devices[12-14], as well as for reversible solid-state hydrogen storage at near ambient conditions[15-19]. This latter proposal, in particular, has motivated great efforts to synthesize and characterize high boron-content graphitic carbon approaching the composition BC_3 as a bulk, free-standing material, in order to assess boron's role in increasing the strength of interaction of graphite-like materials toward H_2.[9, 10, 20]

The first systematic experiments to incorporate boron within graphite were reported by Lowell in 1967 and established the equilibrium limit of boron substitutional doping as 2.35 at. %.[21] Dresselhaus and coworkers investigated boron-implanted graphite (at low doping concentrations) in 1981, elegantly decoupling the effects of substitutional doping as opposed to structural defects (e.g., vacancies) on the Raman spectrum of graphitic carbon.[22] This was followed by a synthetic breakthrough in 1986 when Kouvetakis and coworkers reported a novel route to high boron-content thin-films with a composition of BC_3.[8] This metastable thin-film material was accessed through the reaction of benzene and boron trichloride at relatively low temperatures (800 °C) compared to those required to prepare equilibrium solid solutions (up to 2350 °C). Dahn and coworkers[7, 23], among several other groups[4, 5, 24], were able to reproducibly synthesize and thoroughly characterize similar thin-film materials with tunable compositions up to BC_5. In 2012, Dresselhaus and coworkers followed up previous work by exfoliating low boron-content (equilibrium) graphite to obtain boron-doped graphene (~0.22 at. % substitutional boron) and characterized the materials using Raman spectroscopy.[25] Most recently, bulk graphitic materials of composition ~BC_3 (including some oxygen contamination) have been reported by two synthetic routes: a molecular tiling route based on a single organic precursor[9] and the direct synthesis from a tunable solution of two commercially available liquid precursors[10]. Such materials are free-standing forms of metastable graphitic carbon with a high concentration of boron but also a contribution from oxygen as well as halide contaminants; neither is highly crystalline, but both contain boron chemical environments like that expected for pristine BC_3.

The quantification and characterization of boron inclusion in graphitic carbon is challenging, owing to the fundamental similarities in size and scattering cross-section of boron, carbon, and lattice vacancies. Methods to quantify boron content in carbon-based materials include Auger electron spectroscopy (AES)[7, 23, 24], elastic recoil detection

analysis (ERDA)[10], electron probe microanalysis (EPMA)[5], digestion followed by volumetric titration[21], combustion in fluorine gas to allow for the quantitative detection of BF_3 and CF_4 by IR spectroscopy[8], or by indirect comparison to previous work[22, 26]. Characterization of the boron chemical environment is typically performed by X-ray absorption spectroscopy (XAS)[7], solid-state ^{11}B NMR[9, 10], electron energy-loss spectroscopy (EELS)[27], or X-ray photoelectron spectroscopy (XPS)[9, 25, 28]. This class of materials ranges widely in terms of crystallinity and boron content; the crystalline nature of low boron-content materials reduces the challenge of probing the distinct boron environments. On the other hand, higher concentrations of boron are in all cases inherently accompanied by severe structural disorder and hence characterization is significantly more challenging. In this work we focus on Raman spectroscopy as a versatile and widely available tool for the characterization of high boron-content graphitic materials, and the sensitive relationship it reveals between boron inclusions and defects in the graphitic lattice.

The Raman spectrum of graphite has been a subject of active investigation since 1970 when Tuinstra and Koenig first reported and assigned the E_{2g} Raman-active mode of crystalline graphite, and noticed a lower frequency mode that was only present in defective samples.[29] Several other features, especially a high frequency overtone at ~2700 cm^{-1}, were also observed and discussed, their assignments remaining somewhat disputed for many years owing to the complexity of their physical origin and the unique electronic properties of graphene/graphite. A thorough account of the major developments in and current understanding of the Raman spectrum of graphene and graphite was given by Ferrari and Basko in 2013.[30] Pristine graphite has two formally allowed Raman-active modes, both with E_{2g} symmetry. The most well-known is the higher frequency mode associated with the optical branches of the phonon structure, being degenerate at the Γ point. It arises due to the relative in-plane motion of all sp^2 hybridized carbon atoms, occurring at a Raman shift of ~1580 cm^{-1}, and is commonly referred to as the G mode. The second is a low frequency shearing mode in which the two graphene layers within the unit cell slip with respect to each other, appearing at a Raman shift of ~40 cm^{-1}, and referred to as the C mode. Both vibrational modes occur at the Γ point in the first Brillouin zone where the phonon wavevector is zero, thus satisfying the fundamental Raman selection rule. In addition to these formally allowed modes, more complex resonant processes (enabled by the unusual Dirac cone in the phonon structure of graphene/graphite) can also occur in which electron scattering by defects results in a net conservation of momentum and thus an observed Raman process. This leads to the appearance of a multitude of formally forbidden transitions such as the D, D′, and D′′ modes in graphite that contains defects.[30, 31] These defect-activated modes can provide a wealth of information on the nature and type of defects within graphitic systems. Other combinations and overtone modes involving two such phonons, e.g., the D+D′′, 2D, and 2D′ modes, are also present in the Raman spectrum of graphitic carbon, even in the absence of defects, and become significant due to resonance enhancement. Formally, the individual phonons involved in these combination modes are forbidden due to their non-zero wavevectors; however, when two phonons with opposite wavevectors are combined, momentum can be conserved and the Raman process is observed, resulting in the significant presence of these combination modes even in pristine graphite and graphene when probed at optical incident frequencies.

Changing the excitation energy of the Raman scattering event (a common capability in the modern analytical laboratory) permits the examination of phonon dispersion and other excitation energy-dependent phenomena. It is well known that the position of Raman peaks that originate from double resonance processes, such as the D mode, show a strong dependence on excitation energy.[30, 32, 33] This dispersion relation of the D peak is referred to as Disp(D) and reported in units of cm^{-1} eV^{-1}, the change in observed peak position (Pos(D), in cm^{-1}) as a function of Raman excitation energy (E_L, in eV). The E_L dependence of Pos(D) originates from the slope of the in-plane transverse optical (TO) phonon branch around the Kohn anomaly at the K point in the first Brillouin zone, and is a fundamental material property of the graphitic system. In many materials, this is found to be a linear relation within the typical range of E_L accessible to a benchtop spectrometer[34], providing a convenient metric for assessing the phonon structure of a variety of disordered graphitic materials with varying atomistic structure and composition.

The interpretation of the Raman spectrum of graphite, graphene, and disordered carbon materials is readily extended to graphitic systems containing substitutional boron doping. In such materials, boron doping and structural defects both give rise to the development of the defect-activated D peak. Low boron-content graphitic materials show that even when structural order is unperturbed, the presence of substitutional boron atoms within the graphitic lattice results in a Raman spectrum that is highly influenced by defect-activated modes.[35] By combining information gleaned from other analytical techniques with Raman spectroscopy, it is possible to separate the effects of structural and chemical defects, elucidating the role boron substitution plays on the electronic, vibrational, and physical structure of boron-doped graphitic carbon. In this work, we explore the effect of boron doping within bulk turbostratic graphitic carbon on the phonon dispersion (E_L-dependence) of the D mode.

Using the recently established direct synthesis method,[10] two series of bulk boron-doped graphitic materials were synthesized. The first series focuses on the effect of synthesis temperature: a series of boron-doped graphitic carbon materials with a nominal composition of 25 at. % boron (referred to herein as BC_3′) was synthesized at 750-1100 °C in 50 °C increments. Benzene and tribromobenzene-derived graphitic carbon materials (referred to as C′ and CBr_x′) were also synthesized in a temperature series to elucidate the role of synthesis temperature on the materials properties of boron-free

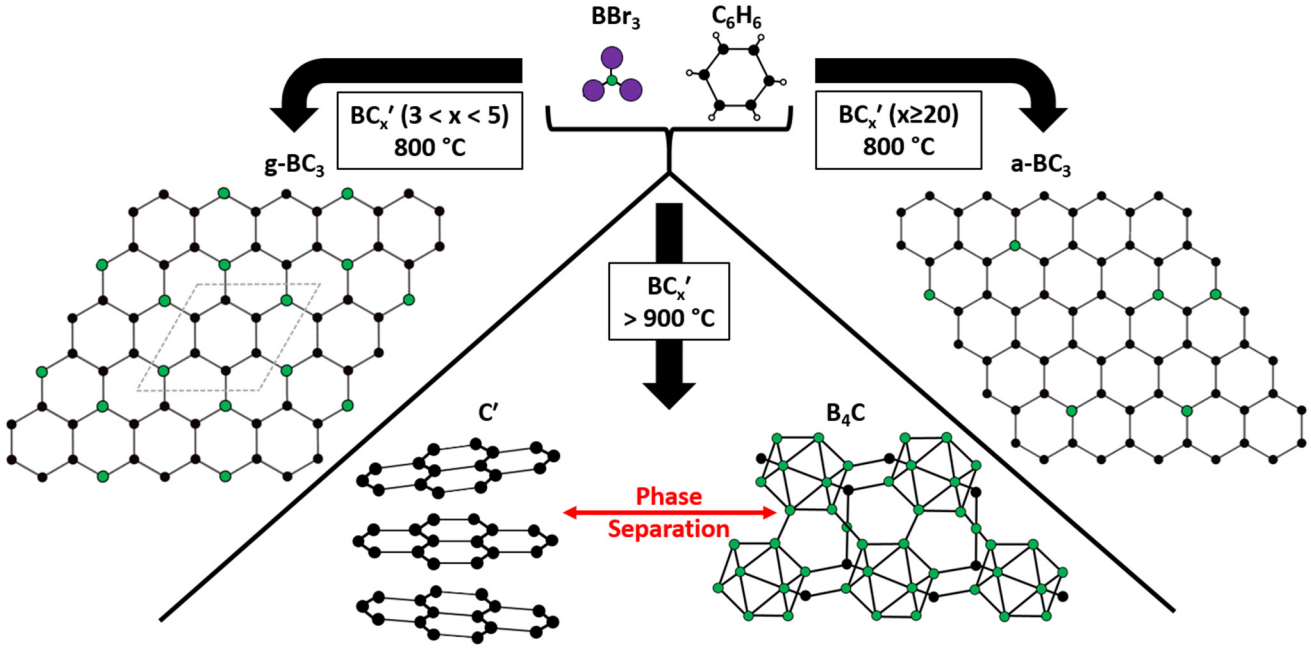

Figure 1. Schematic depiction of the pyrolysis products of boron tribromide and benzene, depending on synthesis temperature and nominal composition (C:B ratio, x). Solid-solutions of boron in turbostratic graphitic carbon are referred to as BC_x' while pure turbostratic graphitic carbon is referred to as C′.

turbostratic carbon, with and without a bromine-containing leaving group. The second series focuses on the effect of boron composition: a series of increasing boron content within turbostratic graphitic carbon (referred to as BC_x') was synthesized at 800 °C, where the nominal composition was varied such that x = 3, 5, 10, 20, 30, and ∞. The material denoted by x = ∞ corresponds to a pure carbon material without any boron precursor (and is hence a variety of C′). Both series were characterized by Raman spectroscopy, as well as several complementary techniques: X-ray diffraction (XRD), Auger electron spectroscopy (AES), energy dispersive X-ray spectroscopy (EDX), and X-ray absorption spectroscopy (XAS). The so-obtained materials of highest importance are summarized in **Figure 1**. Of particular interest is the dispersion of the D peak in the Raman spectrum, and its dependence on the structural and chemical properties of the graphitic lattice. A direct correlation between the presence of ordered BC_3 domains and a reduced phonon dispersion relation of the D peak is observed and corroborated by first-principles calculations of the vibrational structure of high boron-content graphene.

EXPERIMENTAL METHODS

Direct Synthesis of Bulk C′, CBr_x', and BC_x'. A solution of boron tribromide (99.99%, Sigma Aldrich) and benzene (99.8%, Sigma Aldrich), or a neat solution of either benzene or 1,3,5-tribromobenzene (98%, Alfa Aesar), was charged into a quartz ampule (15 cm length, 1 cm inner diameter, closed at one end) inside a glovebox under an inert argon atmosphere (<0.5 ppm of H_2O, <0.5 ppm of O_2). The amounts of the reagents used were determined by selecting the desired stoichiometry (nominal composition) of the product and by limiting the maximum pressure at the synthesis temperature to 20 bar within the quartz ampule, assuming that all of the bromine and/or hydrogen atoms would be evolved as diatomic ideal gases (e.g., 85.1 µL BBr_3 and 40 µL C_6H_6 to achieve a nominal composition of BC_3 in a 14 mL ampule at a maximum temperature of 800 °C). The open end of the ampule was closed with a Swagelok Ultra-Torr adapter and removed from the glovebox. The lower half of the ampule was submerged in liquid nitrogen to solidify the precursors. In this state the ampule was connected to a stainless steel Schlenk line and evacuated to 10^{-2} mbar. The ampule was flame-sealed under active vacuum. The sealed ampule was then placed in the center of a chamber furnace (Carbolite RWF 12/13) and heated to the temperature setpoint (750-1100 °C) via a 1 °C min^{-1} ramp. The set temperature was held for 1 h and then allowed to gradually cool to ambient temperature. The ampule was carefully scored with a diamond-bladed saw and snapped open within a nitrile rubber enclosure, releasing the overpressure of gaseous byproducts into a fume hood. The solid product was collected and washed three times with deionized water, washed three times with acetone, and finally dried in air at 80 °C. The as-synthesized flakes were in some cases investigated without further manipulation or were reduced to powder by ultrasonication in acetone for 5 min prior to drying at 80 °C, as denoted below.

Powder X-ray Diffraction. Powder X-ray diffraction (XRD) was performed on sonicated materials using a Rigaku Ultima IV diffractometer with Cu $K\alpha_{1,2}$ radiation (λ = 1.54 Å) in reflection geometry. Samples were spread thinly on the surface of a zero-background holder constructed of oriented silicon. Analysis of the raw data is described in the Supporting Information.

Raman Spectroscopy. As-synthesized flakes were investigated with a Raman spectrometer (LabRAM HR Evolution, Horiba Scientific Ltd.) equipped with a confocal

microscope and three excitation sources: a 532 nm (2.33 eV) frequency-doubled Nd:YAG laser with an incident power of 10 mW, a 633 nm (1.96 eV) HeNe laser with an incident power of 1.7 mW, and a 785 nm (1.58 eV) diode laser with an incident power of 25 mW. All measurements were performed at room temperature. Analysis of the raw data is described in the Supporting Information.

X-ray Absorption Spectroscopy. The boron and carbon environment of boron-containing materials was examined by X-ray absorption spectroscopy (XAS) using synchrotron radiation at the Advanced Light Source (Lawrence Berkeley National Laboratory). Sonicated samples were mounted on carbon tape and transferred into an ultrahigh vacuum (10^{-9} mbar) chamber for analysis. The total florescence yield (TFY) was measured allowing for probing depths of ~175 nm into the bulk of the sample. Boron oxide (99.999%, Sigma Aldrich), amorphous boron (98%, Alfa Aesar), boron carbide (98%, Sigma Aldrich), and hexagonal boron nitride (99.5%, Alfa Aesar) were also analyzed under the same conditions as standard references. Analysis of the raw data (including additional C K-edge spectra) is described in the Supporting Information.

Elemental Analysis. Auger electron spectroscopy (AES) and energy dispersive X-ray spectroscopy (EDX) were performed using a scanning electron microscope (PHI 710 Scanning Auger NanoProbe, Physical Electronics Inc.) under a highly focused electron beam with a well-defined energy of 10 kV operating at 10 nA. Samples were prepared by pressing the as-synthesized flakes into indium foil. The samples were sputtered for 3 minutes under a 3 keV argon ion beam to clean the surface for AES analysis. For EDX, a windowless X-ray detector (XFlash 6|10, Bruker Corp.) was used, permitting the detection of boron. Analysis of the raw data as well as several representative scanning electron micrographs of the samples are given in the Supporting Information. In the present work, the boron:carbon ratio (e.g., BC_3') is used specifically to indicate the stoichiometry of the initial reaction mixture and is thus the "nominal composition." On the other hand, the measured boron content of a material is reported as a percentage of boron to carbon in molar, dimensionless "at. %.".

Phonon Structure Calculations. Phonon dispersion calculations were performed using plane wave density functional theory (DFT) implemented by the Quantum ESPRESSO package.[36, 37] Rappe-Rabe-Kaxiras-Joannopoulos[38] ultra-soft pseudopotentials were employed to describe the core electrons of carbon and boron. The Perdew-Burke-Ernzerhof (PBE) exchange correlation functional[39] was selected. Supercells consisting of 8 atoms in a single plane were optimized at the PBE level: C_8 (graphene), BC_7, and B_2C_6 (single-layer BC_3). The optimized in-plane lattice constants (a) were found to be 4.930, 5.038, and 5.170 Å, respectively. To minimize the interaction between monolayers, the interlayer lattice constant (c) was set as 15 Å. For the electronic energy calculations and atomic position relaxations, the convergence thresholds were 1×10^{-12} Ry and 1×10^{-7} au, respectively, employing a 16×16×1 k-grid. The phonon dispersion calculations were performed with a 1×10^{-14} Ry threshold, employing an 8×8×1 q-grid. To interpret the phonon behavior of these materials, unfolding of the phonon structure was applied; the unfolded phonon dispersion diagrams reported in this work were generated with the Phonon Unfolding program.[40]

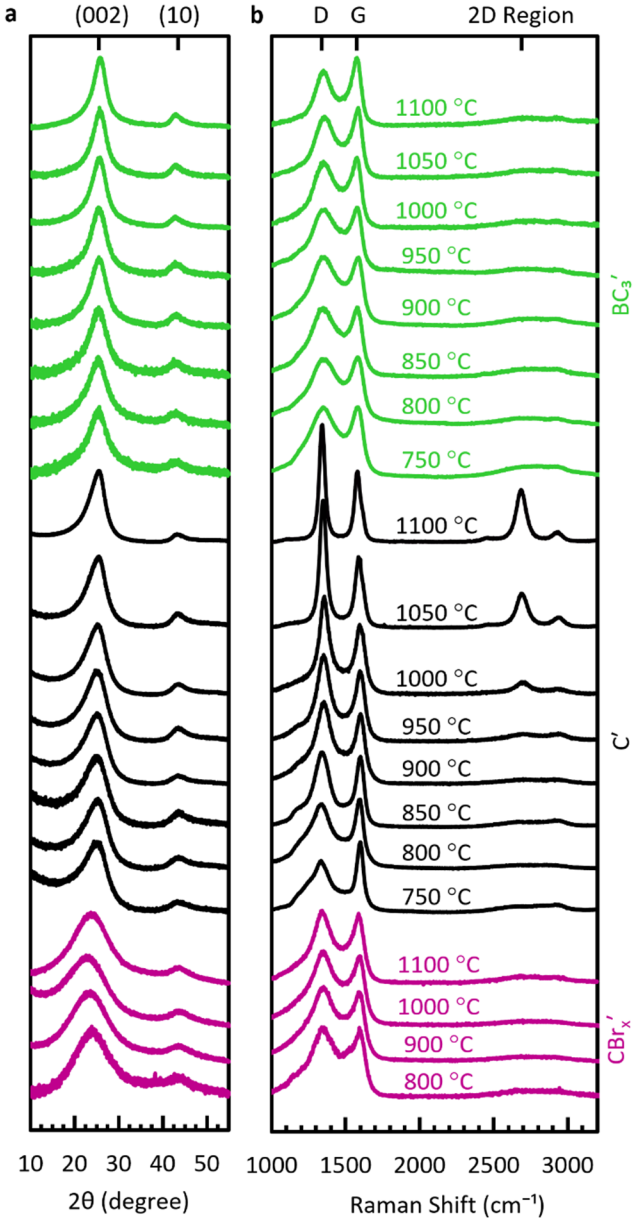

Figure 2. Structural characterization as a function of temperature. (a) XRD patterns and (b) Raman spectra (E_L = 532 nm) of CBr_x' (bottom, magenta), C′ (middle, black), and BC_3' (top, green). Samples were synthesized by the direct method in 50 °C increments between 750-1100 °C.

RESULTS

Structural Characterization. X-ray diffraction patterns and Raman spectra (E_L = 532 nm) of the temperature series of BC_3', C′, and CBr_x' materials synthesized in 50 °C increments ranging from 750 °C to 1100 °C are shown in **Figure 2**. The XRD patterns exhibit two broad reflections

corresponding to a weakly ordered turbostratic graphitic structure: an intense (002) reflection centered between 24-26° and a family of (10) reflections centered at ~43° comprised of (100) and (101) contributions. Tribromobenzene-derived graphitic carbon (CBr_x') exhibits broad (002) and (10) reflections at all synthesis temperatures. This very poor crystallinity is also observed in the broadness of the D and G peaks in the Raman spectrum, where little change is observed over the range of synthesis temperatures explored. Benzene-derived graphitic carbon (C′) exhibits increasing order of the graphitic structure with increasing synthesis temperature, as revealed by a narrowing of the (002) reflection in the XRD patterns. Raman spectroscopy reveals more detailed information about the developing order. The intensity ratio (as defined in the Supporting Information) of the D and G peaks, referred to as I(D)/I(G), is a common metric used to assess the quality of graphitic systems. For turbostratic graphite, an increase in I(D)/I(G), narrowing of all peaks, and the appearance of a well-defined 2D region are evidence of increasing graphitic ordering and the removal of defects within the graphitic lattice.[41] This occurs for all C′ materials synthesized above 950 °C in this work. Interestingly, the BC_3' materials show similar reflections in XRD compared to the C′ materials; yet, their Raman spectra show much more subtle development as a function of increasing synthesis temperature. The I(D)/I(G) of BC_3' decreases with increasing synthesis temperature, opposite to the C′ material, and there is only slight narrowing of both the D and G peaks. Even at the highest synthesis temperature explored (1100 °C), BC_3' does not exhibit a well-defined 2D region.

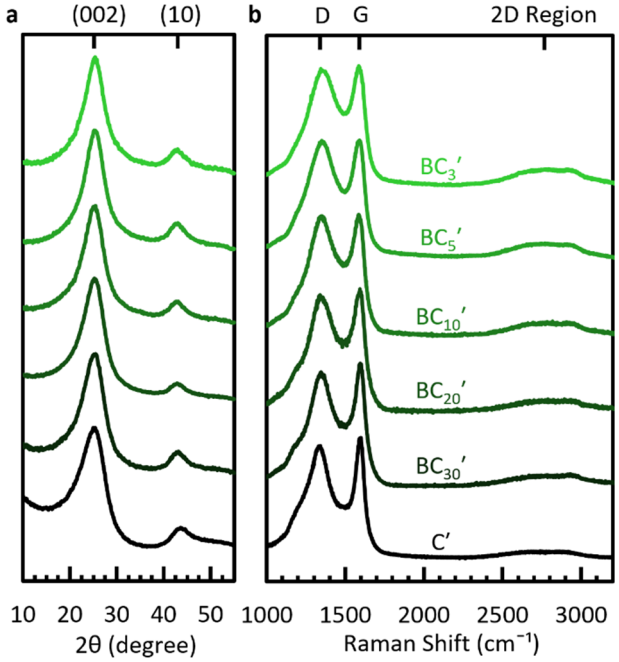

Figure 3. Structural characterization as a function of boron content. (a) XRD patterns and (b) Raman spectra (E_L = 532 nm) of BC_x' (x = 3, 5, 10, 20, 30, and ∞) synthesized by the direct method at 800 °C.

X-ray diffraction patterns and Raman spectra (E_L = 532 nm) of the BC_x' composition series synthesized by the direct method at 800 °C are shown in **Figure 3**. The nominal compositions of BC_x' (x = 3, 5, 10, 20, 30, and ∞) were set by varying the ratio of boron tribromide to benzene in the initial reaction mixture. The XRD patterns of BC_x' do not change significantly with increasing boron content. The Raman spectra, however, show subtle developments as a result of increasing boron concentration. In the absence of boron doping (x = ∞), the D peak is rather pronounced with an obvious shoulder between 1100-1200 cm^{-1}; the G peak is comparatively narrow and the 2D region is broad and very weak. As boron content increases (up to x = 3), both the D and G peaks broaden, and overall intensity in the 2D region increases.

Chemical Composition. The boron content of BC_x' as a function of nominal composition, as independently determined by AES and EDX techniques, is shown in **Figure 4**. The measured boron content is less than the nominal boron content at all compositions. This is likely due to a combination of several effects: incomplete reaction of the boron precursor (BBr_3), side reactions with the quartz ampule during synthesis, formation of soluble boron compounds such as oxide phases, and/or poor boron/carbon resolution inherent to the analytical methods. The latter issue has been remedied in previous work by use of elastic recoil detection analysis (ERDA)[10], an analytical technique that is well-suited to resolving the boron concentration in carbon-based materials based on the signal arising from ^{10}B. In that case, similar materials showed a boron content roughly equivalent to the nominal composition. Nevertheless, in the present work there appears to be a limit to boron incorporation (~12 at. % according to AES and EDX results) reached at the nominal composition of BC_5', corresponding to an actual stoichiometry of ~BC_8. This observation of a limit to boron inclusion at a nominal composition of ~BC_5 is consistent with previous results for thin-film boron-doped graphitic materials.[7]

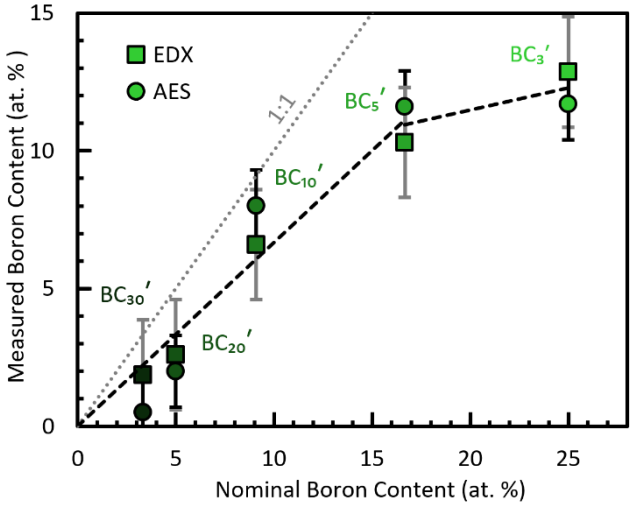

Figure 4. Elemental analysis. Boron content of BC_x' as measured by AES (circles) and EDX (squares) as a function of

nominal composition determined by the B:C ratio of the initial reaction mixture.

Boron Chemical Environment. The boron chemical environments in the BC_3' temperature series and the BC_x' composition series were investigated by XAS, as shown in **Figure 5**. Several standards measured under identical conditions, as well as relevant literature references, are shown in **Figure 5a** to represent the possible chemical bonding environments in directly synthesized BC_x'. Boron oxide exhibits a very strong absorption associated with the σ* transition of the BO_3 type boron environments at 193.7 eV. Amorphous boron shows a broad, featureless absorption edge with an onset at 187-190 eV. Boron carbide (B_4C) exhibits a characteristic absorption associated with the σ* transition of icosahedral boron environments at 190.6 eV. Hexagonal boron nitride, in polycrystalline powder form, shows a strong absorption associated with the π* transition of trigonal planar BN_3 type boron at 191.6 eV, and a weaker absorption associated with the σ* transition between 197-200 eV. The XAS spectrum of a thin-film material of reported composition $B_{0.25}C_{0.75}$ (TF-BC_3) is also shown for comparison; this spectrum was originally reported by Caretti and coworkers in 2008[42], and later reinterpreted by Pallier and coworkers in 2013[43]. Four distinct boron environments are present in TF-BC_3: in ascending energy, Pallier et al. interpret these as trigonal planar mixed $BC_{3-x}B_x$ environments in an amorphous lattice labeled as a-BC_3 (189.4 eV), an icosahedral B_4C-like environment (190.6 eV), a trigonal planar BC_3 environment with long range graphitic order labeled g-BC_3 (192.0 eV), and a boron oxide environment (193.7 eV). The g-BC_3 environment was also observed by Way and coworkers in their studies of thin-film BC_x, the intensity of which was shown to depend on the angle of incidence.[7] This supports the assignment of this peak as being due to a π* transition in a graphitic lattice with long range order (similar to oriented pristine graphite which shows a π* transition that exhibits strong angular dependence[42, 44]). All XAS spectra of boron-containing materials exhibit at least a weak contribution from BO_3 type boron environments consistent with the boron oxide standard.

The boron K-edge region of the XAS spectrum of the BC_3' temperature series synthesized between 750-1100 °C is shown in **Figure 5b** and enlarged in **Figure 5e**. Boron oxide environments can be seen in all samples, most likely due to a surface oxide layer present on the sonicated materials, formed during handling. The material synthesized at 750 °C shows little evidence of boron-carbon bonding. The BC_3' materials synthesized between 800-900 °C show a distinct g-BC_3 environment as well as a minor contribution from a-BC_3 environments. Between 950-1050 °C, the g-BC_3 environment becomes less distinguishable due to greater spectral weight from a broad feature corresponding to boron carbide environments. At 1100 °C, the g-BC_3 structure is completely obscured by the presence of B_4C as well as two other environments (marked with asterisks) that appear at 191.3 and 193.0 eV which have not yet been assigned. These latter contributions are suspected to be related to sub-stoichiometric boron carbide domains.[43]

The boron K-edge region of the XAS spectrum of the BC_3' temperature series and BC_x' composition series is shown in **Figure 5b-c** and enlarged in **Figure 5d-e**. Three boron environments can be seen in all samples with varying intensities as a function of boron content. As above, boron oxide environments are present in all samples. The material with the lowest boron content (of nominal composition BC_{30}) shows a contribution from a-BC_3 type environments and no contribution from g-BC_3. The ratio of g-BC_3 to a-BC_3 increases as a function of nominal boron content with the peak intensity ratio reaching ~1:1 in BC_{10}'. At the nominal compositions of BC_5 and BC_3, the g-BC_3 environment dominates, indicating that ordering is more developed with respect to the graphitic lattice for directly synthesized BC_5' and BC_3'. Overall, XAS analysis has shown that g-BC_3 environments are most prevalent in BC_x' synthesized between 800-950 °C; further heating results in phase separation into low boron-content graphitic material and boron carbide. At low boron compositions (x = 20 and 30), a-BC_3 environments are prevalent, by increasing boron content, spectral weight is shifted from a-BC_3 to g-BC_3 environments with extended hexagonal order.

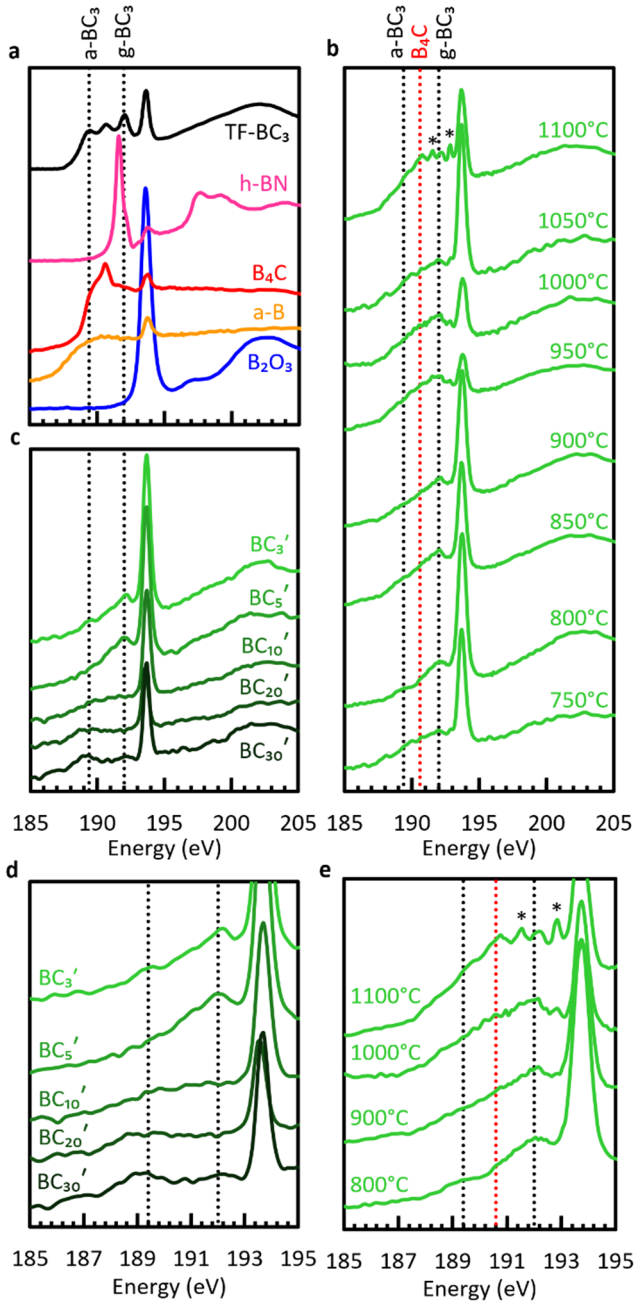

Figure 5. Boron chemical environment. XAS spectra near the B K-edge of BC_x' synthesized by the direct method and related materials: (a) boron oxide, amorphous boron, and hexagonal boron nitride, chosen as standards, and thin film BC_3 (TF-BC_3) as a literature reference[43], (b) BC_x' composition series, and (c) BC_3' temperature series. The near edge region is expanded for (d) the BC_x' composition and (e) BC_3' temperature series.

DISCUSSION

X-ray diffraction, Raman spectroscopy, and X-ray absorption spectroscopy of boron-doped graphitic carbon synthesized by the direct method (BC_x') combine to yield an illuminative picture as to the interplay between structural defects (e.g., vacancies, edge sites, and stacking mismatch) and boron substitutions on overall disorder within the graphitic lattice. For BC_x' materials, X-ray diffraction probes atomic periodicities without significant regard for elemental composition (boron and carbon have similar atomic form factors toward X-rays). Meanwhile, Raman spectroscopy is highly sensitive to bonding symmetry and therefore to elemental composition within the underlying graphitic lattice, the unique Raman spectrum of graphite especially so. A peculiarity of the characterization of graphitic carbon materials by Raman spectroscopy is that the resonance enhancement effect (which occurs at all excitation energies) renders any other present phases less prominent in the measured spectrum. Therefore, non-crystalline secondary phases may remain undetected by both XRD and Raman characterization; this is addressed herein by X-ray absorption spectroscopy, which reveals all boron-containing chemical environments in each material.

X-Ray Diffraction. The evolution of the underlying graphitic structural regularity of BC_x', C′, and CBr_x' as a function of boron content or synthesis temperature as revealed by X-ray diffraction is shown in **Figure 6**. The average d_{002} spacing was determined by applying Bragg's law to the position of the (002) reflection. The average crystallite size along the c and a axes, referred to as L_c and L_a respectively, were estimated by applying the Scherrer equation to the full-width at half-maximum (FWHM) of the (002) and (100) reflections.[45] Further details related to XRD pattern analysis can be found in the Supporting Information. The effects of temperature on the graphitic structure of directly synthesized BC_3', C′, and CBr_x' are shown in **Figures 5a-c**. Directly-synthesized BC_3' exhibits the largest graphitic crystallites (in both L_c and L_a) and simultaneously the smallest d_{002} spacing (closest to pristine graphite). With an increase in synthesis temperature, the crystallites become larger and exhibit narrower interlayer spacing. Hence, the average number of layers per crystallite is the highest for BC_3' synthesized at 1100 °C: ~6 layers per crystallite. Pure graphitic carbon derived from benzene (C′) also exhibits measurable increases in L_c and L_a as synthesis temperature increases, although with less change in the interlayer spacing. For C′, the maximum number of layers per crystallite is also observed for the material synthesized at 1100 °C: ~5 layers per crystallite. Hence, XRD analysis confirms that BC_x' is, overall, more ordered than C′ synthesized by the same method.

The CBr_x' materials exhibit the weakest ordering (smallest crystallite size) and the largest interlayer spacing of all the materials investigated: >3.7 Å. CBr_x' was investigated to assess the effect of bromine as opposed to hydrogen on the structure of the resulting graphitic materials. The low crystallinity of CBr_x' confirms that the presence of boron within the reaction mixture to produce BC_x' is responsible

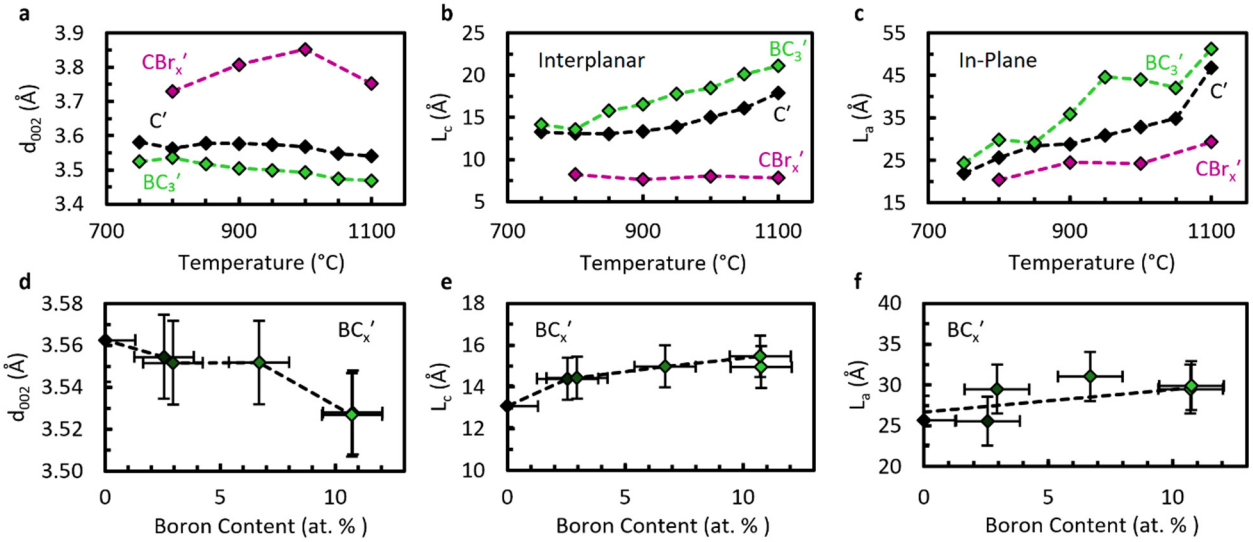

Figure 6. Interlayer spacing and crystallite size. The development of (a) d_{002}, (b) L_c, and (c) L_a as a function of synthesis temperature within the BC_3', C′, and CBr_x' temperature series. The development of (d) d_{002}, (e) L_c, and (f) L_a as a function of boron content measured by AES within the BC_x' composition series.

for its higher crystallinity (consistent with earlier results[46, 47]), and contradicts that the presence of bromine in the boron precursor drives the reaction toward a higher crystalline graphitic product. This issue had previously hindered the direct comparison of non-halide precursor-derived pure carbon materials (e.g., C′) with boron trihalide-derived materials (e.g., BC_x') which always exhibit higher crystallinity under equivalent synthesis conditions. The graphitic structure of the composition series, BC_x' synthesized at 800 °C is shown in **Figures 5d-f**. An increase in L_c and L_a (15% and up to 20%, respectively) are observed as a function of boron content, this catalytic effect of boron on the formation of graphite is consistent across literature.[11, 46, 47] The average d_{002} spacing is ~3.55 Å for all nominal compositions up to BC_{10} (corresponding to measured boron contents of <10 at. %) and decreases to ~3.53 Å for BC_5' and BC_3' (corresponding to measured boron contents of ~12 at. %). The reduction in d_{002} spacing between BC_{10}' and BC_5' is directly correlated with the evolution of the g-BC_3 environments observed by XAS (see **Figure 5d**). Although the d_{002} spacing in directly synthesized BC_x' is larger than that of high boron-content thin films prepared by CVD methods (3.48-3.34 Å), the trend of decreasing interlayer spacing with increasing boron content remains consistent with previous observations for both equilibrium solid-solutions of boron in graphite as well as disordered boron-doped graphitic materials.[7, 21, 23, 48]

Raman Spectroscopy. Further insights into the graphitic structure as well as the role of chemical defects were deduced by analysis of the Raman spectrum of BC_x' as compared to C′ and CBr_x'. Four simple metrics to describe structural development/deterioration within the graphitic carbon amorphization trajectory proposed by Ferrari and Robertson[41] were extracted from each individual Raman spectrum, as shown in **Figure 7**. The first metric described in their work is the intensity ratio of the D and G peaks, referred to as I(D)/I(G). As graphitic carbon degrades from crystalline graphite (stage 1) to defective turbostratic graphite (stage 2) and eventually into amorphous carbon (stage 3), I(D)/I(G) is non-monotonically related to graphitic ordering. It first increases as a result of interruptions in symmetry of the graphitic lattice, resulting in an increase in the number of 6-fold rings that have been isolated from the bulk by defects. I(D)/I(G) reaches a maximum at the transition from stage 1 to stage 2, and then decreases as 6-fold rings are destroyed in the material. This is due to the opening of 6-fold rings into chains that only express the formally allowed Raman-active G mode. The second metric is the (apparent) position of the G peak, referred to as Pos(G), observed at ~1580 cm^{-1} for pristine graphite (stage 1). As defects are introduced and the crystallites reduce in size, Pos(G) increases to ~1600 cm^{-1} for turbostratic graphite at the transition from stage 1 to stage 2. This is a result of an increasing FWHM(G) combined with the appearance of the neighboring defect-activated D′ mode at ~1620 cm^{-1}; the merging of these two peaks results in an apparent shift in Pos(G) to higher frequencies for turbostratic graphite. If the material degrades further into amorphous carbon (stage 3), the D′ mode is no longer active due to the total destruction of the graphitic structure, resulting in an apparent reversal in the shift of Pos(G). The third and fourth metrics are the FWHM of the D and G peaks, referred to as FWHM(D) and FWHM(G), respectively. FWHM(D) and FWHM(G) always increase with increasing defects and disorder, making it possible to distinguish between stage 1 and stage 2 of the proposed amorphization trajectory. When boron is incorporated into the graphite lattice, local symmetry around each lattice site is broken, resulting in the appearance of "defect-activated" modes and the broadening of features even when the lattice is pristinely ordered. At first, this seems to be an inconvenience as substitutional dopants lend a similar contribution to the Raman spectrum as defects. However, when the Raman spectrum

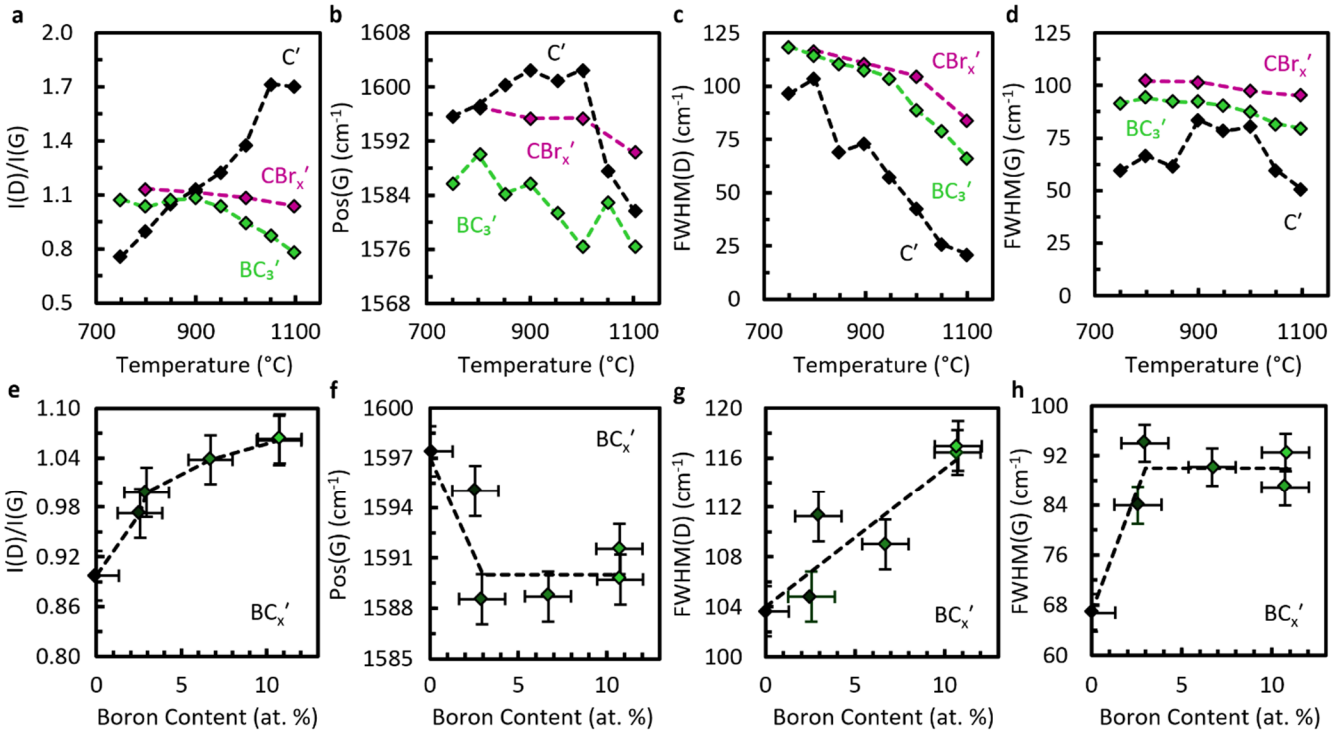

Figure 7. Raman spectroscopy analysis (E_L = 532 nm). The (a) I(D)/I(G) ratio, (b) Pos(G), (c) FWHM(D), and (d) FWHM(G) as a function of synthesis temperature within the BC_3', C′, and CBr_x' temperature series. The (e) I(D)/I(G) ratio, (f) Pos(G), (g) FWHM(D), and (h) FWHM(G) as a function of measured boron content by AES within the BC_x' composition series.

of BC_3' is compared to that of C′ and the results are combined with structural and chemical information obtained by XRD and XAS, the two contributions (boron doping vs. lattice defects) can be effectively decoupled.

Temperature and Graphitic Structure. Analysis of the Raman spectra of the BC_3', C′, and CBr_x' temperature series as well as the BC_x' composition series by the aforementioned four metrics is shown in **Figures 6a-d**. The I(D)/I(G), Pos(G), and FWHM(D) of the low temperature variants of C′ indicate it to be stage 2 nanocrystalline graphitic carbon, referring to the stages of the amorphization trajectory as proposed by Ferrari and Robertson.[41] Directly synthesized C′ undergoes a transition to stage 1 nanocrystalline graphitic carbon as synthesis temperature is increased. This is determined by the maximum reached in I(D)/I(G) as well as in Pos(G) and is corroborated by examining the crystallite size along the c axis as determined by XRD, where L_c increases from 1.3 to 1.7 nm. Interestingly, BC_3' does not show the same maximum in I(D)/I(G) and Pos(G) even though the crystallite size in the c axis is larger, increasing from 1.4 to 2.1 nm with increasing synthesis temperature. This can be explained by the high boron content within the graphitic lattice that presents as substitutional defects, resulting in a Raman spectrum that reflects a more disordered system compared to its C′ counterparts, despite having larger crystallites as detected by XRD. There is a reduction in FWHM(D) with increasing synthesis temperature for all samples, indicating an overall ordering of the material at higher temperatures. The decrease in FWHM(D) for the C′ materials is roughly linear over the entire temperature range with a slope of -24 cm^{-1} per 100 °C. The BC_3' material shows two distinct regions for the evolution of FWHM(D). Between 750 and 950 °C, FWHM(D) changes little with synthesis temperature, having a slope of -7 cm^{-1} per 100 °C. However, from 950 to 1100 °C the D peak narrows at the same rate as the C′ materials, having a slope of -24 cm^{-1} per 100 °C. Hence, this is an important transition temperature that indicates significantly different structural properties of directly-synthesized BC_3'; at 950 °C and above, the material transitions into graphitic carbon with similar spectral behavior as found in boron-free graphitic carbon.

The above results indicate that boron leaves the graphitic BC_x' phase at high temperatures, whereupon temperature plays a similar role in improving the graphitic ordering, as for the C′ counterparts. The same two regions are also observed for the CBr_x' material. This is proposed to be a result of bromine atoms that have not been expelled from the material until it is heated above 950 °C. It is known that bromine forms stable intercalation compounds within graphite.[49,50] This process is only partially reversible in that the last 5-10% of the intercalated bromine can only be removed by strong heating to form volatile carbon derivatives that incorporate bromine.[51] In the present work, intercalated bromine and its destructive deintercalation process likely explains the larger d_{002} and low values of L_c and L_a observed over the CBr_x' temperature series as seen in **Figure 6a-c**.

Boron Content and Graphitic Structure. The effect of boron doping within the graphitic lattice on key features of the Raman spectra of the BC_x' composition series are shown in **Figures 6e-h**. The overall effect is an increased ordering

as a result of increasing boron content, being consistent with previous studies of boron-doped graphitic thin-films.[23] This is most clearly observed by inspection of Pos(G) (**Figure 7f**); Pos(G) initially decreases with increasing boron content and then settles at ~1590 cm^{-1}. Hence, low boron content BC_x' initially exhibits a nanocrystalline graphitic structure near the transition from stage 2 to stage 1 of the amorphization trajectory, shifting further into stage 1 for $x \leq 20$. This trend is corroborated by XRD analysis, showing a decrease in d_{002} and an increase in L_c and L_a as a function of increasing boron content (**Figures 5d-f**). Despite increasing ordering, increasing boron content results in an increase in I(D)/I(G), until the composition saturates (at ~12 at. % boron as measured by AES) as shown in **Figure 7e**. This is a direct result of boron incorporation within the material, as the substitutional boron atoms act as defects that break symmetry and activate the D mode.[23] The G mode, on the other hand, arises from the relative motion of all sp^2-hybridized lattice site occupants and its intensity is not expected to be greatly affected by boron content. Hence, an increasing I(D)/I(G) with increasing boron content is associated exclusively with an increased contribution from the D mode that has been activated by substitutional boron atoms. FWHM(D) also increases with boron content due to an increase in the number and type of defects (e.g., a-BC_3, $BC_{3-x}B_x$, g-BC_3, or BO_3). Lastly, FWHM(G) increases as a function of boron content, which can be explained by two phenomena: increasing intensity of the D′ peak that presents as a high frequency shoulder of the G peak and the difference in mass of boron and carbon that leads to slight perturbations of the phonon frequency.[23]

Phonon Dispersion Relation. Many features of the Raman spectrum of graphitic materials are sensitively dependent on the excitation energy, E_L. In particular, I(D)/I(G) increases as excitation energy decreases (see **Figure S2b**).[34, 52, 53] This significantly changes the appearance of the Raman spectrum and emphasizes that I(D)/I(G) is only a useful metric for the comparison of graphitic materials when measured with the same E_L. Of particular interest in this work is the E_L dependence of Pos(D), a relation referred to as Disp(D) that probes the phonon structure of the highest optical branch around the K point. In highly crystalline graphitic systems, the introduction of a low concentration of defects leads to a well-defined Disp(D) of 50-60 cm^{-1} eV^{-1}.[54] Similar values of Disp(D) are observed across a plethora of other graphitic systems exhibiting a variety of defect types and concentrations.[25, 34] The dispersion of the D peak is a result of the steep slope of the Kohn anomaly located on the TO phonon branch near the first Brillouin zone corner K (see **Figure S7**). On the other hand, the TO branch for single-layer BC_3, the highest boron content investigated in this work, shows no evidence for a Kohn anomaly at the K point, and it would therefore be expected that pure, crystalline BC_3 exhibits no dependence of Pos(D) on excitation energy, E_L.

The phonon dispersion relation of the D peak in the BC_3' temperature series and the BC_x' composition series is shown in **Figure 8**. Boron-free materials (C′ and CBr_x') and low boron-content materials (BC_x' with x = 20 and 30) show a Disp(D) of ~45-55 cm^{-1} eV^{-1}. Similarly, BC_3' materials synthesized at ≥ 1000 °C exhibit a dispersion of ~55 cm^{-1} eV^{-1} or larger. On the other hand, BC_3' materials synthesized at 950 °C or lower exhibit a distinctly lower Disp(D), between 30-40 cm^{-1} eV^{-1}. It should be noted that the dispersion of the G peak in all materials was found to be ~0, supporting the classification of these materials as stage 1 and 2 graphitic carbon in the Ferrari amorphization trajectory, comprised primarily of sp^2 hybridize lattice sites.[41]

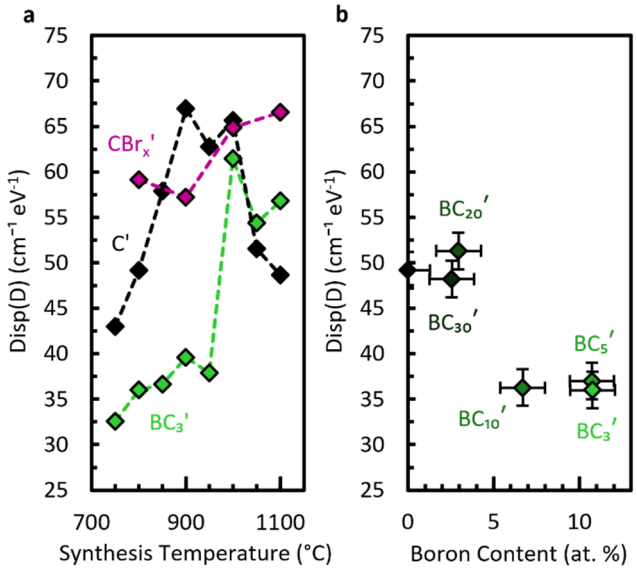

Figure 8. Phonon dispersion of the D mode. (a) The Disp(D) as a function of synthesis temperature for BC_3', C′, and CBr_x' temperature series materials. (b) The Disp(D) as a function of measured boron content within the BC_x' composition series synthesized at 800 °C.

The temperature series of CBr_x' materials was examined to determine if the presence of bromine is a cause of the observed shift in Disp(D). However, these materials show an even higher Disp(D) of ~60 cm^{-1} eV^{-1} over the entire temperature range studied herein. This demonstrates that the presence of bromine is not responsible for the unusually low Disp(D) of the BC_3' materials synthesized at or below 950 °C. The C′ materials do have a somewhat lower dispersion of ~43 cm^{-1} eV^{-1} when synthesized at very low temperatures (only at 750 °C in this work). However, such materials are poorly crystalline and exhibit a D peak that is not well defined (a broad low-energy shoulder complicates the fitting analysis). At 800 °C, the Disp(D) of C′ is ~50 cm^{-1} eV^{-1} and further heating to 1000 °C continues to increase the Disp(D) to a maximum of ~65 cm^{-1} eV^{-1}, similar to highly defected CBr_x'. Above 1000 °C, the Disp(D) of C′ returns to ~50 cm^{-1} eV^{-1}, as expected for typical forms of nanocrystalline graphitic carbon.

Unlike C′ and CBr_x', directly-synthesized BC_3' has an unusually low Disp(D) of ~30-40 cm^{-1} eV^{-1} when synthesized between 750-950 °C, as seen in **Figure 8a**. This temperature range favors a prevalence of trigonal planar g-BC_3 environments (as evidenced by XAS, **Figure 5e**). Hence, g-BC_3 environments are likely responsible for the distinctly low value of Disp(D) observed in high boron-content BC_x' synthesized at or below 950 °C. At or above 1000 °C, the

boron in any would-be g-BC_3 environments is subject to phase separation into low boron-content graphitic domains (with < 3 at. % B) and boron carbide, as indicated by XAS. The low boron-content, disordered graphitic carbon exhibits a Disp(D) of ~50 cm^{-1} eV^{-1}, consistent with many other varieties of graphitic carbon. Disp(D) as a function of boron content for the BC_x' materials synthesized at 800 °C is shown in **Figure 8b**. At low boron compositions (x = 20 and 30), Disp(D) is ~50 cm^{-1} eV^{-1}. According to XAS results, the boron in these materials is mainly comprised of a-BC_3 environments (**Figure 5d**) that do not have a large influence on the phonon structure of the graphitic nanocrystals. At higher boron compositions (x = 10, 5, and 3), Disp(D) is ~36 cm^{-1} eV^{-1} and g-BC_3 is the dominant boron carbon bonding environment indicated by XAS (**Figure 5d**).

A reduced Disp(D) of 37 cm^{-1} eV^{-1} has also been observed for highly ordered boron-doped graphene produced by the exfoliation of equilibrium solid-solution boron doped graphite formed at 2450 °C (corresponding to a substitutional boron content of 0.22 at. %). This effect can be explained by electron hole doping of the pristine graphene lattice, resulting from the dilute presence of electron deficient boron substitutions.[25, 55] The high boron content in bulk BC_x' produced herein, however, prohibits an explanation of the reduced Disp(D) due to hole doping.[55] Instead, DFT calculated phonon dispersion diagrams of single-layer BC_3 reveal a ring breathing mode with similar A_{1g} symmetry to the well-known D mode in graphite/graphene (see **Figures S7-S8**). This phonon originates from a flat optical branch around K resulting in a lower observed Disp(D) for the breathing mode in BC_3' (which exhibits a mixed character between BC_3 and pure graphite). The breathing mode in BC_3 is also calculated to exhibit a higher frequency than the D mode in graphite, resulting in an increase in Pos(D) at all E_L, in excellent agreement with experimental results (see **Figure S2b**). The Disp(D) of 30-40 cm^{-1} eV^{-1} observed in BC_3', BC_5', and BC_{10}' can be explained by a hindered phase separation of the developing metastable material, and therefore the presence of a significant population of g-BC_3 structures that are required to exhibit the phonons responsible for the distinctly lower value of Disp(D). In BC_{20}' and BC_{30}', the concentration of boron is not sufficient to form g-BC_3 units under the synthesis conditions explored; instead there is a random distribution of a-BC_3 within the graphitic lattice that exhibits the standard D mode of defected boron-free graphite. Once the boron concentration reaches a threshold, observed herein between BC_{20}' and BC_{10}', the majority of the boron exists in g-BC_3 domains that facilitate the phonon responsible for the observed dispersion relation of ~30-40 cm^{-1} eV^{-1}.

CONCLUSIONS

Directly synthesized bulk boron-doped graphitic carbon exhibits a uniquely reduced D peak dispersion relation of 30-40 cm^{-1} eV^{-1} when the concentration of boron within the graphitic lattice exceeds ~3 at. %, a condition that favors ordered, trigonal planar BC_3 chemical environments. This has been confirmed by complementary X-ray diffraction, Raman spectroscopy, and X-ray absorption spectroscopy studies that decouple the effects of boron doping on the structure and composition of the underlying lattice. The unique, metastable phase of high boron-content graphitic carbon is only accessible between synthesis temperatures of 800-950 °C; at temperatures of ≥ 1000 °C, a phase separation between boron carbide and the graphitic solution occurs, resulting in a leaching of boron from the graphitic phase. Bulk graphitic materials prepared without substitutional boron (or with undetectable quantities of g-BC_3 environments), while exhibiting many similar features in their respective X-ray diffraction patterns and Raman spectra, exhibit a higher D peak dispersion relation of ~50 cm^{-1} eV^{-1}, characteristic of common graphite. Hence, the D peak dispersion can be used to uniquely identify bulk graphitic materials with a substitutional boron content approaching BC_3, which are of high interest in applications ranging from hydrogen storage to lithium-ion batteries.

ASSOCIATED CONTENT

Supporting Information

Data analysis methods, scanning electron microscopy, and phonon structure calculations. This material is available free of charge via the Internet at http://pubs.acs.org.

AUTHOR INFORMATION

Corresponding Author

*nstadie@montana.edu

Author Contributions

The manuscript was written through contributions of all authors.

ACKNOWLEDGMENTS

We thank Nicholas J. Borys for insightful discussions. Acknowledgement is made to the donors of the American Chemical Society Petroleum Research Fund for support of this research. We thank the Montana Nanotechnology Facility (MONT, an NNCI facility supported by National Science Foundation grant ECCS-1542210) for the use of their instrumentation. We acknowledge research support from the U.S. Department of Energy (DOE), Office of Energy Efficiency and Renewable Energy, Fuel Cell Technologies Office through the Hydrogen Storage Materials Advanced Research Consortium (HyMARC). This research employed resources of the Advanced Light Source (Beamline 8.0.1) which is a DOE Office of Science User Facility under Contract No. DE-AC02-05CH11231. Portions of this work were performed under the auspices of the DOE by Lawrence Livermore National Laboratory under Contract No. DE-AC52-07NA27344.

REFERENCES

(1) Breckenridge, R. G. *Thermoelectric Materials Final Report*. Union Carbide Corp.: Parma, OH, **1960**.

(2) Woodley, R. E. The Oxidation of Boronated Graphite. *Carbon* **1968**, 6, 617-626.

(3) Fecko, D. L.; Jones, L. E.; Thrower, P. A. The formation and oxidation of BC_3, a new graphitelike material. *Carbon* **1993**, 31, 637-644.

(4) Cermignani, W.; Paulson, T. E.; Onneby, C.; Pantano, C. G. Synthesis and Characterization of Boron-Doped Carbons. *Carbon* **1995**, 33, 367-374.
(5) Shirasaki, T.; Derré, A.; Ménétrier, M.; Tressaud, A.; Flandrois, S. Synthesis and characterization of boron-substituted carbons. *Carbon* **2000**, 38, 1461-1467.
(6) Davidson, J. M.; Gates, L. O.; Nightingale, R. E. Radiation-Damage Effects in Borated Graphite. *Nucl. Sci. Eng.* **1966**, 26, 90-98.
(7) Way, B. M.; Dahn, J. R.; Tiedje, T.; Myrtle, K.; Kasrai, M. Preparation and characterization of B_xC_{1-x} thin films with the graphite structure. *Phys. Rev. B* **1992**, 46, 1697-1702.
(8) Kouvetakis, J.; Kaner, R. B.; Sattler, M. L.; Bartlett, N. A novel graphite-like material of composition BC_3, and nitrogen–carbon graphites. *J. Chem. Soc., Chem. Commun.* **1986**, 1758-1759.
(9) King, T. C.; Matthews, P. D.; Glass, H.; Cormack, J. A.; Holgado, J. P.; Leskes, M.; Griffin, J. M.; Scherman, O. A.; Barker, P. D.; Grey, C. P.; et al. Theory and practice: bulk synthesis of C_3B and its H_2- and Li-storage capacity. *Angew. Chem. Int. Ed.* **2015**, 54, 5919-5923.
(10) Stadie, N. P.; Billeter, E.; Piveteau, L.; Kravchyk, K. V.; Döbeli, M.; Kovalenko, M. V. Direct Synthesis of Bulk Boron-Doped Graphitic Carbon. *Chem. Mater.* **2017**, 29, 3211-3218.
(11) Endo, M.; Kim, C.; Karaki, T.; Nishimura, Y.; Matthews, M. J.; Brown, S. D. M.; Dresselhaus, M. S. Anode performance of a Li ion battery based on graphitized and B-doped milled mesophase pitch-based carbon fibers. *Carbon* **1999**, 37, 561-568.
(12) Liu, Y.; Artyukhov, V. I.; Liu, M.; Harutyunyan, A. R.; Yakobson, B. I. Feasibility of Lithium Storage on Graphene and Its Derivatives. *J. Phys. Chem. Lett.* **2013**, 4, 1737-1742.
(13) Joshi, R. P.; Ozdemir, B.; Barone, V.; Peralta, J. E. Hexagonal BC3: A Robust Electrode Material for Li, Na, and K Ion Batteries. *J. Phys. Chem. Lett.* **2015**, 6, 2728-2732.
(14) Fitzhugh, W.; Li, X. Modulation of Ionic Current Limitations by Doping Graphite Anodes. *J. Electrochem. Soc.* **2018**, 165, A2233-A2238.
(15) Zhang, C.; Alavi, A. Hydrogen absorption in bulk BC_3: a first-principles study. *J. Chem. Phys.* **2007**, 127, 214704.
(16) Firlej, L.; Kuchta, B.; Wexler, C.; Pfeifer, P. Boron substituted graphene: energy landscape for hydrogen adsorption. *Adsorption* **2009**, 15, 312.
(17) Zhu, Z. H.; Lu, G. Q.; Hatori, H. New Insights into the Interaction of Hydrogen Atoms with Boron-Substituted Carbon. *J. Phy. Chem. B* **2006**, 110, 1249-1255.
(18) Sha, X.; Cooper, A. C.; Bailey, W. H.; Cheng, H. Revisiting Hydrogen Storage in Bulk BC_3. *J. Phys. Chem. C* **2010**, 114, 3260-3264.
(19) Nayyar, I.; Ginovska, B.; Karkamkar, A.; Gennett, T.; Autrey, T. Physi-Sorption of H_2 on Pure and Boron–Doped Graphene Monolayers: A Dispersion–Corrected DFT Study. *C* **2020**, 6, 15.
(20) Bult, J. B.; Lee, J.; O'Neill, K.; Engtrakul, C.; Hurst, K. E.; Zhao, Y.; Simpson, L. J.; Parilla, P. A.; Gennett, T.; Blackburn, J. L. Manipulation of Hydrogen Binding Energy and Desorption Kinetics by Boron Doping of High Surface Area Carbon. *J. Phys. Chem. C* **2012**, 116, 26138-26143.
(21) Lowell, C. E. Solid Solution of Boron in Graphite. *J. Am. Ceram. Soc.* **1967**, 50, 142-144.
(22) Elman, B. S.; Dresselhaus, M. S.; Dresselhaus, G.; Maby, E. W.; Mazurek, H. Raman scattering from ion-implanted graphite. *Phys. Rev. B* **1981**, 24, 1027-1034.
(23) Naeini, J. G.; Way, B. M.; Dahn, J. R.; Irwin, J. C. Raman scattering from boron-substituted carbon films. *Phys. Rev. B* **1996**, 54, 144-151.
(24) Kouvetakis, J.; McElfresh, M. W.; Beach, D. B. Chemical vapor deposition of highly conductive boron-doped graphite from triphenyl boron. *Carbon* **1994**, 32, 1129-1132.
(25) Kim, Y. A.; Fujisawa, K.; Muramatsu, H.; Hayashi, T.; Endo, M.; Fujimori, T.; Kaneko, K.; Terrones, M.; Behrends, J.; Eckmann, A.; et al. Raman Spectroscopy of Boron-Doped Single-Layer Graphene. *ACS Nano* **2012**, 6, 6293-6300.
(26) Hagio, T.; Nakamizo, M.; Kobayashi, K. Studies on X-ray diffraction and Raman spectra of B-doped natural graphite. *Carbon* **1989**, 27, 259-263.
(27) Serin, V.; Brydson, R.; Scott, A.; Kihn, Y.; Abidate, O.; Maquin, B.; Derré, A. Evidence for the solubility of boron in graphite by electron energy loss spectroscopy. *Carbon* **2000**, 38, 547-554.
(28) Kim, E.; Oh, I.; Kwak, J. Atomic structure of highly ordered pyrolytic graphite doped with boron. *Electrochem. Commun.* **2001**, 3, 608-612.
(29) Tuinstra, F.; Koenig, J. L. Raman Spectrum of Graphite. *J. Chem. Phys.* **1970**, 53, 1126-1130.
(30) Ferrari, A. C.; Basko, D. M. Raman spectroscopy as a versatile tool for studying the properties of graphene. *Nat. Nanotechnol.* **2013**, 8, 235.
(31) Dresselhaus, M. S.; Jorio, A.; Saito, R. Characterizing Graphene, Graphite, and Carbon Nanotubes by Raman Spectroscopy. *Annu. Rev. Condens. Matter Phys.* **2010**, 1, 89-108.
(32) Thomsen, C.; Reich, S. Double Resonant Raman Scattering in Graphite. *Phys. Rev. Lett.* **2000**, 85, 5214-5217.
(33) Maultzsch, J.; Reich, S.; Thomsen, C.; Requardt, H.; Ordejón, P. Phonon Dispersion in Graphite. *Phys. Rev. Lett.* **2004**, 92, 075501.
(34) Matthews, M. J.; Pimenta, M. A.; Dresselhaus, G.; Dresselhaus, M. S.; Endo, M. Origin of dispersive effects of the Raman D band in carbon materials. *Phys. Rev. B* **1999**, 59, 6585-6588.
(35) Endo, M.; Hayashi, T.; Hong, S.-H.; Enoki, T.; Dresselhaus, M. S. Scanning tunneling microscope study of boron-doped highly oriented pyrolytic graphite. *J. Appl. Phys.* **2001**, 90, 5670-5674.
(36) Giannozzi, P.; Baroni, S.; Bonini, N.; Calandra, M.; Car, R.; Cavazzoni, C.; Ceresoli, D.; Chiarotti, G. L.; Cococcioni, M.; Dabo, I.; et al. QUANTUM ESPRESSO: a modular and open-source software project for quantum simulations of materials. *J. Phys. Condens. Mat.* **2009**, 21, 395502.
(37) Giannozzi, P.; Andreussi, O.; Brumme, T.; Bunau, O.; Buongiorno Nardelli, M.; Calandra, M.; Car, R.; Cavazzoni, C.; Ceresoli, D.; Cococcioni, M.; et al. Advanced capabilities for

materials modelling with Quantum ESPRESSO *J. Phys. Condens. Mat.* **2017**, 29, 465901.

(38) Rappe, A. M.; Rabe, K. M.; Kaxiras, E.; Joannopoulos, J. D. Optimized pseudopotentials. *Phys. Rev. B* **1990**, 41, 1227-1230.

(39) Perdew, J. P.; Burke, K.; Ernzerhof, M. Generalized Gradient Approximation Made Simple. *Phys. Rev. Lett.* **1996**, 77, 3865-3868.

(40) Zheng, F.; Zhang, P. Phonon Unfolding: A program for unfolding phonon dispersions of materials. *Comput. Phys. Commun.* **2017**, 210, 139-144.

(41) Ferrari, A. C.; Robertson, J. Interpretation of Raman spectra of disordered and amorphous carbon. *Phys. Rev. B* **2000**, 61, 14095-14107.

(42) Caretti, I.; Gago, R.; Albella, J. M.; Jiménez, I. Boron carbides formed by coevaporation of B and C atoms: Vapor reactivity, B_xC_{1-x} composition, and bonding structure. *Phys. Rev. B* **2008**, 77, 174109.

(43) Pallier, C.; Leyssale, J.-M.; Truflandier, L. A.; Bui, A. T.; Weisbecker, P.; Gervais, C.; Fischer, H. E.; Sirotti, F.; Teyssandier, F.; Chollon, G. Structure of an Amorphous Boron Carbide Film: An Experimental and Computational Approach. *Chem. Mater.* **2013**, 25, 2618-2629.

(44) Brühwiler, P. A.; Maxwell, A. J.; Puglia, C.; Nilsson, A.; Andersson, S.; Mårtensson, N. π^* and σ^* Excitons in C 1s Absorption of Graphite. *Phys. Rev. Lett.* **1995**, 74, 614-617.

(45) Langford, J. I.; Wilson, A. J. C. Scherrer after sixty years: A survey and some new results in the determination of crystallite size. *J. Appl. Crystallogr.* **1978**, 11, 102-113.

(46) Murty, H. N.; Biederman, D. L.; Heintz, E. A. Apparent catalysis of graphitization. 3. Effect of boron. *Fuel* **1977**, 56, 305-312.

(47) Oya, A.; Yamashita, R.; Otani, S. Catalytic graphitization of carbons by borons. *Fuel* **1978**, 58.

(48) Turnbull, J. A.; Stagg, M. S.; Eeles, W. T. Annealing studies of boron-doped graphite by electron microscopy and X-ray diffraction. *Carbon* **1966**, 3, 387-392.

(49) Young, D. A. The intercalation process in graphite-bromine. *Carbon* **1977**, 15, 373-377.

(50) Chung, D. D. L. Structure and phase transitions of graphite intercalated with bromine. *Phase Transit.* **1986**, 8, 35-57.

(51) Lancette, J.-M.; Roussel, R. Metals intercalated in graphite. V. A concentration cell with intercalated bromine. *Can. J. Chem.* **1976**, 54, 4.

(52) Sood, A. K.; Gupta, R.; Asher, S. A. Origin of the unusual dependence of Raman D band on excitation wavelength in graphite-like materials. *J. Appl. Phys.* **2001**, 90, 4494-4497.

(53) Ferrari, A. C.; Robertson, J. Resonant Raman spectroscopy of disordered, amorphous, and diamondlike carbon. *Phys. Rev. B* **2001**, 64, 075414.

(54) Pócsik, I.; Hundhausen, M.; Koós, M.; Ley, L. Origin of the D peak in the Raman spectrum of microcrystalline graphite. *J. Non-Cryst. Solids* **1998**, 227-230, 1083-1086.

(55) Attaccalite, C.; Wirtz, L.; Lazzeri, M.; Mauri, F.; Rubio, A. Doped Graphene as Tunable Electron−Phonon Coupling Material. *Nano Lett.* **2010**, 10, 1172-1176.
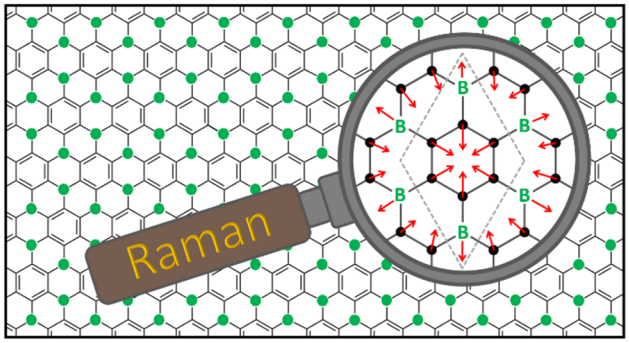
TOC graphic